

FAST Observations of Four Comets to Search for the Molecular Line Emissions between 1.0 and 1.5 GHz Frequencies

Long-Fei Chen^{1,2,3}, Chao-Wei Tsai^{4,5,6}, Jian-Yang Li⁷, Bin Yang⁸, Di Li^{3,4,9}, Yan Duan¹⁰, Chih-Hao Hsia¹¹, Zhichen Pan⁴, Lei Qian⁴, Donghui Quan³, Xue-Jian Jiang³, Xiaohu Li¹², Ruining Zhao^{13,14}, and Pei Zuo⁴ School of Physics and Electronic Science, Guizhou Normal University, Guiyang 550025, China ² Guizhou Provincial Key Laboratory of Radio Astronomy and Data Processing, Guiyang 550025, China Research Center for Astronomical Computing, Zhejiang Laboratory, Hangzhou 311100, China ⁴ National Astronomical Observatories, Chinese Academy of Sciences, Beijing 100101, China; cwtsai@nao.cas.cn Institute for Frontiers in Astronomy and Astrophysics, Beijing Normal University, Beijing 102206, China ⁶ Key Laboratory of Radio Astronomy and Technology, Chinese Academy of Sciences, Beijing 100101, China School of Atmospheric Sciences, Sun Yat-sen University, Zhuhai 519082, China ⁸ Núcleo de Astronomía, Facultad de Ingenieríay Ciencias, Universidad Diego Portales, Chile ⁹ Department of Astronomy, College of Physics and Electronic Engineering, Qilu Normal University, Jinan 250200, China Department of Electronic and Optical Engineering, Space Engineering University, Beijing 101416, China Laboratory for Space Research, Faculty of Science, The University of Hong Kong, Hong Kong (SAR), China Xinjiang Astronomical Observatory, Chinese Academy of Sciences, Urumqi 830011, China ¹³ CAS Key Laboratory of Optical Astronomy, National Astronomical Observatories, Chinese Academy of Sciences, Beijing 100101, China School of Astronomy and Space Sciences, University of Chinese Academy of Sciences, Beijing 100049, China Received 2024 April 22; revised 2024 August 29; accepted 2024 September 5; published 2024 October 2

Abstract

We used the Five-hundred-meter Aperture Spherical radio Telescope (FAST) to search for the molecular emissions in the *L*-band between 1.0 and 1.5 GHz toward four comets, C/2020 F3 (NEOWISE), C/2020 R4 (ATLAS), C/2021 A1 (Leonard), and 67P/Churyumov-Gerasimenko during or after their perihelion passages. Thousands of molecular transition lines fall in this low-frequency range, many attributed to complex organic or prebiotic molecules. We conducted a blind search for the possible molecular lines in this frequency range in those comets and could not identify clear signals of molecular emissions in the data. Although several molecules have been detected at high frequencies of greater than 100 GHz in comets, our results confirm that it is challenging to detect molecular transitions in the *L*-band frequency ranges. The non-detection of *L*-band molecular lines in the cometary environment could rule out the possibility of unusually strong lines, which could be caused by the masers or non-LTE effects. Although the line strengths are predicted to be weak, for FAST, using the ultra-wide bandwidth receiver and improving the radio frequency interference environments would enhance the detectability of those molecular transitions at low frequencies in the future.

Key words: astrochemistry - ISM: molecules - comets: general - line: identification

1. Introduction

Comets are considered "fossils" of our solar system according to the planet formation theories (Shu 1977; Brasser & Morbidelli 2013). Following the formation of the Solar Nebula from molecular cloud to protostar and protoplanetary disk, planetesimals formed and finally evolved to the present day solar system (Ehrenfreund & Charnley 2000; Chambers 2023). Thus, the composition of comets may reflect the initial environments of our solar system (van Dishoeck et al. 2013; Willacy et al. 2022). For example, the various molecular species detected in the cometary coma may have inherited from the protosolar nebula (Bergner & Ciesla 2021), where they are frozen onto and preserved in the ice mantles of the dust grains until the comets travel to inner solar system to the Sun to release the species into the gas phase under solar heating.

The composition of comets offers a useful chemical way to study the molecular inheritance from the Solar Nebula's evolutionary history. More than 70 molecules have been identified from various comets by remote or in situ measurements (Rubin et al. 2019), with 67P/Churyumov–Gerasimenko having the highest number of discovered molecules (Biver & Bockelée-Morvan 2019) from measurements by the Rosetta mission, including both simple species such as hydroxyl (Smith et al. 2021), and complex species such as glycine (Altwegg et al. 2016).

Besides the identification of molecules by in situ mass spectrometer measurements and by electron excitation in ultraviolet and visible wave ranges, the rotationally excited transitions of the gas-phase molecules located in the (sub-)millimeter frequency range provide the best way to detect them remotely by radio observations to reveal the kinetics and excitation conditions of the environment where these molecules are located. For example, using Atacama Large Millimeter/Submillimeter Array (ALMA), Roth et al. (2021) detected the emissions from

Table 1				
Observing Conditions of the Four Comets Observed by FAST				

Comet Name	Start Observing UT time	Magnitude (mag)	Heliocentric Distance (AU)	Geocentric Distance (AU)	$\frac{\dot{\Delta}^{a}}{(\text{km s}^{-1})}$
	O1 time	(mag)	Distance (AU)	Distance (AU)	(KIII S)
C/2020 F3 (NEOWISE)	2020-08-01 06:15	5.9	0.827	0.793	35.84
C/2020 R4 (ATLAS)	2021-03-31 23:30	13.9	1.138	0.947	-49.86
C/2020 R4 (ATLAS)	2021-04-02 23:30	13.9	1.152	0.890	-49.31
C/2020 R4 (ATLAS)	2021-04-29 14:30	13.5	1.400	0.506	27.80
C/2020 R4 (ATLAS)	2021-04-30 14:30	13.6	1.411	0.522	31.37
67P/C-G	2021-10-18 20:30	10.1	1.225	0.442	-3.74
67P/C-G	2021-11-02 19:30	10.0	1.211	0.421	-1.26
C/2021 A1 (Leonard)	2021-12-07 00:40	5.3	0.846	0.326	-49.00

Note

methanol, formaldehyde, and other species from comet C/2015 ER61 (PanSTARRS) in the radio frequency around ~ 350 GHz, revealing the low coma kinetic temperature and its asymmetric expansion velocity. Bergman et al. (2022) detected the methanol and hydrogen cyanide in several comets using the Onsala 20 m telescope at a frequency near 90 GHz, revealing short-time activity variations of those comets.

Although many observations of molecular transitions have been reported in the 10 GHz and higher frequency range, the lower frequency range is under-explored, and the molecules detected in these bands only represent a small fraction of the molecules detected in comets. Detection of molecular transitions in the low-frequency ranges is challenging. Salter et al. (2008) conducted a line search within a bandwidth between 1.1 and 10 GHz using the Arecibo Telescope toward the starburst galaxy, Arp 220. Several absorption lines were reported, with their rest frequencies all above 4 GHz. Only one absorption feature around 1.638 GHz was found, which was attributed to ¹⁸OH or formic acid (HCOOH) due to line confusion. Tan et al. (2020) performed surveys toward star-forming regions to search for molecular lines in the frequency range 6.0-7.4 GHz using the same telescope, resulting in the detection of only three molecules, CH₃OH, H₂CS, and OH. In the low frequencies down to 1 GHz of the radio L-band, only the OH 18 cm Λ -doublet transitions have been detected for many comets using the Arecibo Telescope, Nançay Radio Telescope, and Green Bank Telescope (Lovell et al. 2002; Tseng et al. 2007; Smith et al. 2021; Drozdovskaya et al. 2023). At even lower frequencies around 0.1 GHz, tentative detection of NO and its isotopologues, t-DCOOH, ¹⁷OO, as well as SH were reported toward Galactic Center and Orion using the Murchison Widefield Array (Tremblay et al. 2017, 2018, 2020).

The Five-hundred-meter Aperture Spherical radio Telescope (FAST) is the world's largest single-dish radio telescope with three times the sensitivity of the Arecibo Telescope (Nan et al. 2011; Li et al. 2018; Qian et al. 2020). Thus, it provides a great

opportunity to search for molecules in the frequency range from 1.0 to 1.5 GHz with its 19-beam receiver. In this paper, we report the first attempt to search for molecular lines in four comets observed by FAST in 2020 and 2021. The observational setups are presented in Section 2. Sections 3 and 4 discuss the results and the interpretations, respectively. We reach our conclusions in Section 5.

2. Observations

Four comets were observed from 2020 August to 2021 December, including three long-period comets, C/2020 F3 (NEOWISE) (hereafter NEOWISE, Bauer et al. 2020; Biver et al. 2022), C/2020 R4 (ATLAS) (Manzini et al. 2021), and C/2021 A1 (Leonard) (Leonard et al. 2021; Zhang et al. 2021), and one Jupiter-family comet, 67P/Churyumov-Gerasimenko (hereafter 67P/C-G) (Biver et al. 2023). Table 1 summarizes the observation log. The Ephemeris of each comet was obtained from the HORIZONS system of Jet Propulsion Laboratory (Giorgini et al. 1996). All comets were moving at less than 15' per minute during the tracking, well within the 30' per minute tracking limit of FAST (Jiang et al. 2020). The observations of comet NEOWISE were conducted during the gap between two maintenance periods of FAST when the comet was near its closest approach to Earth, and the observations of other comets were Target of Opportunity (ToO) observations. Table 2 lists the FAST programs to observe these comets.

For comet NEOWISE, the target was observed with 12 observation blocks, each with an on-source integration time of 10 minutes in a tracking observation mode centered in the central beam (M01) of the FAST 19-beam receiver. To obtain off-source measurement for baseline subtraction, every four on-source observation schedules were accompanied by an observation schedule at $\sim 3^{\circ}$ from the target. Pulsar and spectral data were simultaneously recorded in the FAST backend during the observations. The pulsar data were used to search for pulsar

^a Line-of-sight velocity of the target with respect to the observer. A positive value means the target center is moving away from the observer, negative indicates movement toward the observer. Data were taken from JPL/Horizons ephemeris.

 Table 2

 Receiver Configurations for our Observations of the Four Comets

Comet Name	Duration	Noise Injection Period (Seconds, cal-on +	Program ID
	(minutes)	cal-off)	
C/2020 F3	120	2 (1 + 1)	
(NEOWISE)			
C/2020 R4 (ATLAS)	65	10(0.1+9.9)	PT2020_0166
C/2020 R4 (ATLAS)	65	10(0.1+9.9)	PT2020_0166
C/2020 R4 (ATLAS)	220	10(0.1+9.9)	PT2020_0166
C/2020 R4 (ATLAS)	210	10(0.1+9.9)	PT2020_0166
67P/C-G	120	8(1+7)	PT2021_0045
67P/C-G	90	8(1+7)	PT2021_0045
C/2021 A1 (Leonard)	120	8(1+7)	PT2021_0045

Note. The dates of observations for these comets are in Table 1. The PIs of these observations are Zhichen Pan for comet NEOWISE, Chao-Wei Tsai for program ID PT2020_0166, and Zhong-Yi Lin for program ID PT2021_0045, respectively.

candidates with no positive detections (Pan et al. 2021; Qian & Pan 2021). The spectral data were used in this work to search for molecular lines from the comet. It should be noted that for the tracking mode used for comet NEOWISE, the comet was actually not tracked. The telescope pointing was targeted at a fixed R.A. and decl. coordinate that was consistent with the position of the comet NEOWISE during each observation block. However, due to the moving speed is faster for comet than for background stars, the comet would move out of the beam after a period of time. Thus, the tracking time for comet NEOWISE was limited to 10 minutes at each observation block to ensure the comet remained within the 2'.9 (at 1.4 GHz) beam size of M01. The left panel of Figure 2 shows the optical image of comet NEOWISE taken at the site of FAST during the observations.

For the other three comets that we observed, a custom observation mode was developed in order to improve the observational efficiency for moving targets. Compared with the tracking mode used for comet NEOWISE, these three comets were tracked at their non-sidereal rates in this custom mode, i.e., their R.A. and decl. coordinates were update in real time. In this mode, the target comet was placed at the central beam M01 and the side beam M11 of the 19-beam receiver alternatively with a 5 minutes integration in each beam. This new mode would allow one beam to acquire the source signal while the other simultaneously acquires the off-source sky background. When alternating between two beams, the source can be continuously observed, although the sky subtraction has to be performed for each beam individually because different beams have different gains. For our observations, the separation of 10/22 between M01 and M11 required 30 s to switch between them to avoid exceeding the acceleration limit of 90" per second for the FAST receiver maneuver. Figure 1 shows the tracking positions and the orbital coordinates of comet C/2020 R4 (ATLAS) on 2021 April 30. The right panel of Figure 2 shows its optical image centered at the M01 beam and overlaid by the FAST 19-beam receiver.

Table 2 summarizes the observation setups. The spectral backend with 1,048,576 channels was configured to cover 1.0–1.5 GHz at a frequency resolution of 476.8 Hz, corresponding to a velocity resolution of 0.1 km s⁻¹ at 1.420 GHz. The sampling time was 1 s for the observations on comet NEOWISE and 0.1 s for other comets. The flux calibration utilized the noise diode with an injection to the optical path in the low-intensity mode (1 K) for NEOWISE and the high-intensity mode (10 K) for other comets. The noise injection period varied for different comets, as listed in Table 2. Assuming a system temperature of 24 K (Jiang et al. 2020) and an hour of integration, the rms noise level could reach 13 mK.

3. Data Processing and Analysis

The receiver recorded the full polarization of the signal in the backend during the observations. We first averaged the total power in the two perpendicular polarization directions, and converted the total power to antenna temperature using Equation (1),

$$T_{\rm a} = T_{\rm noise} \times \frac{{\rm Power_{cal-off}}}{{\rm Power_{cal-on} - Power_{cal-off}}},$$
 (1)

where $T_{\rm noise}$ is the temperature of noise injection, and Power_{cal-on} and Power_{cal-off} are the total power when the noise injection was switched on and off, respectively. From the spectra for CH₃OH (Figure 3), we can see that the rms of the final spectrum is consistent with the estimated noise level.

3.1. Molecular Line Searching

To search for the molecular transition lines in the L-band, we collected a list of lines from the Splatalogue¹⁵ database in the frequency range from 1.0 to 1.5 GHz. We carried out a systematic blind search based on the prospective molecular lines in selected frequency ranges without strong radio frequency interference (RFI). Table 3 shows examples of the prospective molecular transition lines for CH_3OH and ^{17}OH in the L- band.

Methanol is one of the common ice components and has been detected in a number of comets (Rubin et al. 2019). Figures 3 and 4 show our spectra that cover the expected CH₃OH lines for comets 67P/C-G and C/2021 A1 (Leonard), respectively. However, no clear methanol emissions are discernible. A suspicious signal of CH₃OH at 1.120 GHz for comet C/2021 A1 (Leonard) is visible in Figure 4. However, it is present in both the on-source and off-source observations for

¹⁵ https://splatalogue.online/

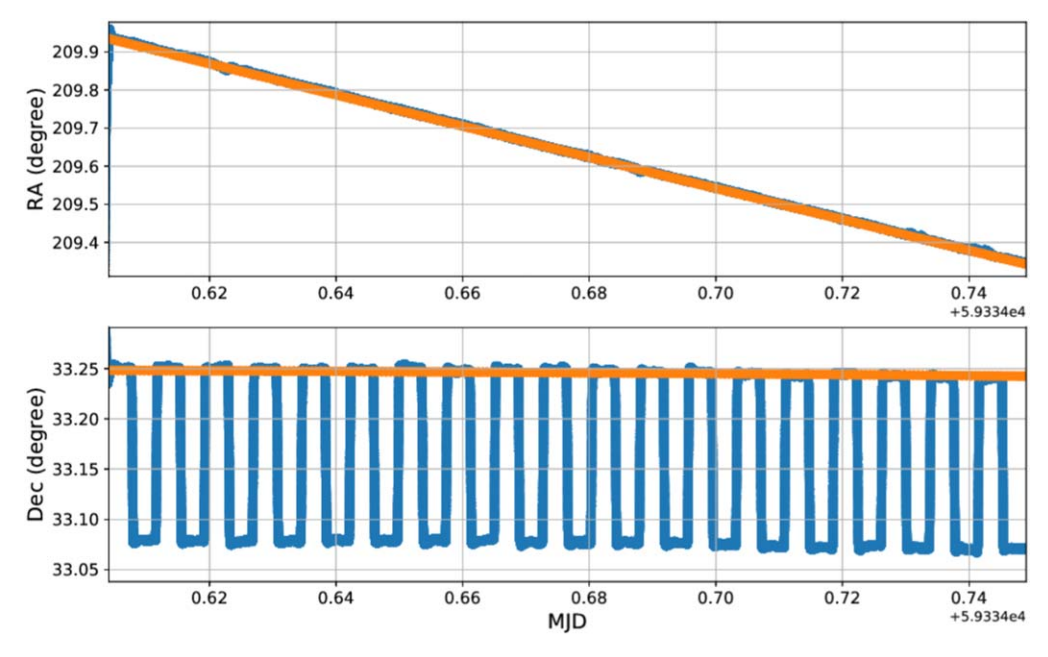


Figure 1. The telescope tracking (blue) and the actual R.A. and decl. coordinates (orange) for comet C/2020 R4 (ATLAS) on 2021 April 30.



Figure 2. (a) The image of comet NEOWISE stacked with 20 pictures, each with an exposure of 30 s. It was taken with a 127 mm refraction telescope at the FAST site on 2020 July 30. (b) The $25' \times 23'$ optical image of comet C/2020 R4 (ATLAS) from Lulin observatory taken on 2021 April 30 overlaid with the beam positions of the FAST 19-beam receiver.

both beam M01 and beam M11 and therefore is most likely RFI. Assuming a rotation temperature of 36 K and a line width of $0.7 \, \mathrm{km \, s^{-1}}$ for the methanol emission as indicated by the IRAM 30 m observations (Biver et al. 2023), the estimated 3σ upper limit production rate of CH₃OH at 1.443 GHz for 67P/C-G is 2×10^{32} molecules s⁻¹ for two hours of integration time using the equation from Drahus et al. (2010). Compared with the derived production rate of CH₃OH (around

 10^{26} molecules s⁻¹) from Biver et al. (2023), this estimated upper limit is too high to give a reasonable constrains. Due to the non-detection of molecular lines, we therefore constrained the integrated intensity of CH₃OH at 1.443 GHz based on its reported production rate and described the results in the later section.

The 18 cm OH line has been detected in many comets in the L-band by the Arecibo Telescope, Nançay Radio Telescope, and

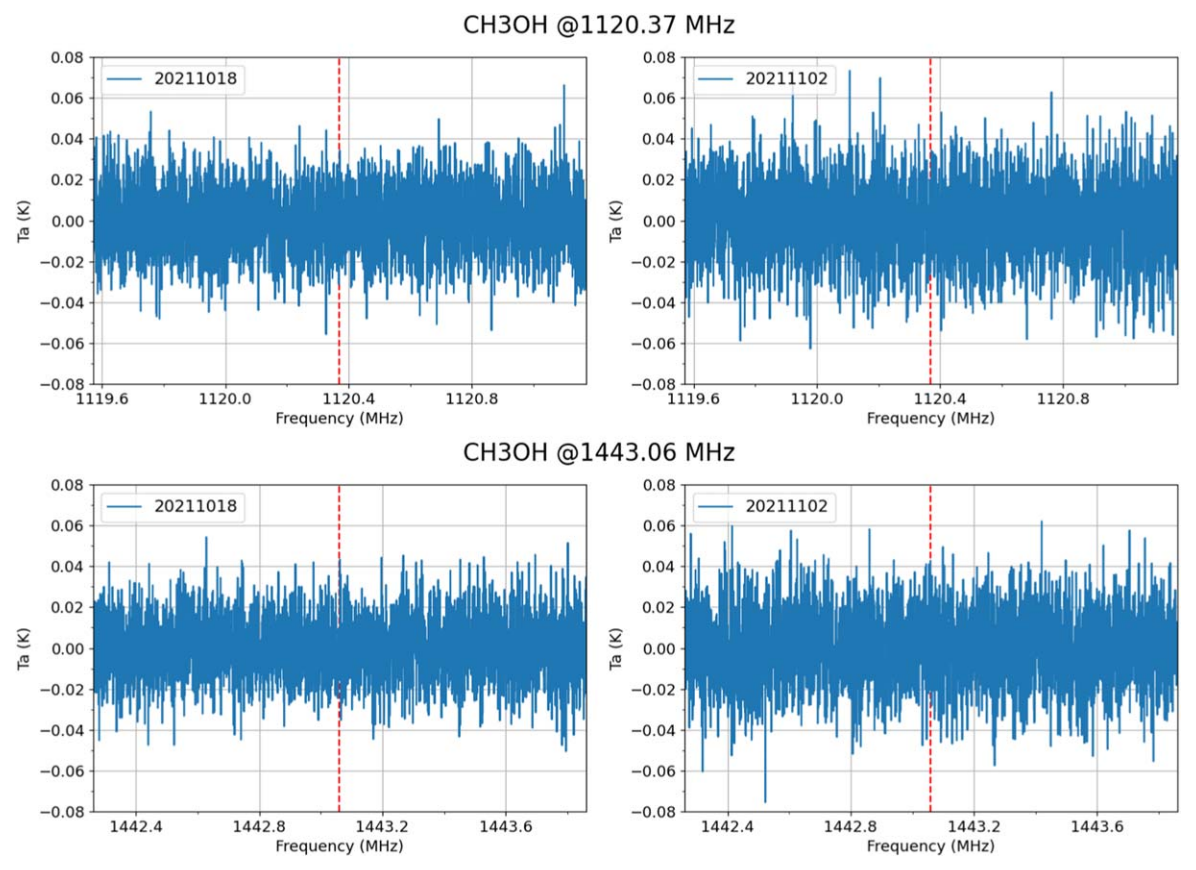


Figure 3. The spectra of comet 67P/C-G obtained on 2021 October 18 and 2021 November 02. The red vertical dashed lines mark the rest frequencies of CH_3OH . The upper and lower panels are for CH_3OH at 1.120 and 1.443 GHz, respectively.

Molecule	Quantum Numbers (Lower–Upper)	Rest Frequency (MHz)	$ \log_{10}A_{ij} \\ (s^{-1}) $	$E_{\rm up}$ (K)	$S_{ij}\mu^2$ (Debye ²)
CH ₃ OH	10(2, 8) - 10(2, 9) A, vt = 0 5(1, 4) - 5(1, 5) A, vt = 1	1120.3700 1443.0600	-12.35144 -12.04136	165.40152 360.02069	2.28465 1.14368
¹⁷ OH	$N = 5-5$, $J+1/2 = 9/2 - 9/2$, $p = 11$, $F_1 = 4-4$, $F+1/2 = 3/2-3/2$	1004.7774	-12.39136	872.65326	0.13758
	$N = 5-5$, $J+1/2 = 9/2-9/2$, $p = 11$, $F_1 = 5-5$, $F+1/2 = 5/2-5/2$	1051.5782	-12.33068	872.65681	0.20702
	$N = 1-1$, $J+1/2 = 3/2-3/2$, $p = -1-1$, $F_1 = 1-2$, $F+1/2 = 5/2-3/2$	1073.217	-13.76028	0.10158	0.00724
	$N = 5-5$, $J+1/2 = 9/2-9/2$, $p = 11$, $F_1 = 5-4$, $F+1/2 = 5/2-3/2$	1076.7262	-13.60391	872.65672	0.01028
	$N = 1-1$, $J+1/2 = 3/2-3/2$, $p = -1-1$, $F_1 = 1-2$, $F+1/2 = 7/2-7/2$	1132.5617	-12.50549	0.07795	0.14774
	$N = 1-1$, $J+1/2 = 3/2-3/2$, $p = -1-1$, $F_1 = 1-1$, $F+1/2 = 5/2-3/2$	1302.1124	-10.81113	0.10163	3.60695
	$N = 1-1$, $J+1/2 = 3/2-3/2$, $p = -1-1$, $F_1 = 2-2$, $F+1/2 = 7/2-5/2$	1322.4597	-10.77313	0.10318	5.01041
	$N = 1-1$, $J+1/2 = 3/2-3/2$, $p = -1-1$, $F_1 = 1-2$, $F+1/2 = 3/2-1/2$	1418.1976	-10.78143	0.11943	1.99290
	$N = 1-1$, $J+1/2 = 3/2-3/2$, $p = -1-1$, $F_1 = 1-2$, $F+1/2 = 3/2-3/2$	1445.0345	-11.22889	0.11942	0.67236
	$N = 1-1$, $J+1/2 = 3/2-3/2$, $p = -1-1$, $F_1 = 2-2$, $F+1/2 = 5/2-3/2$	1455.7225	-10.62898	0.11993	3.92646
	$N = 1-1$, $J+1/2 = 3/2-3/2$, $p = -1-1$, $F_1 = 1-2$, $F+1/2 = 3/2-1/2$	1475.8429	-11.52867	5125.78645	0.31647

Green Bank Telescope (Lovell et al. 2002; Tseng et al. 2007; Smith et al. 2021; Drozdovskaya et al. 2023). Unfortunately, the OH transitions at 1.665 and 1.667 GHz are out of the frequency range of the FAST *L*-band receiver. However, several tens of

 17 OH transitions and six 18 OH transitions are located within the FAST L-band receiver. Figure 5 shows those spectra for comet C/2021 A1 (Leonard). Again, no 17 OH and 18 OH transitions are visible in our data. However, there is a suspicious absorption

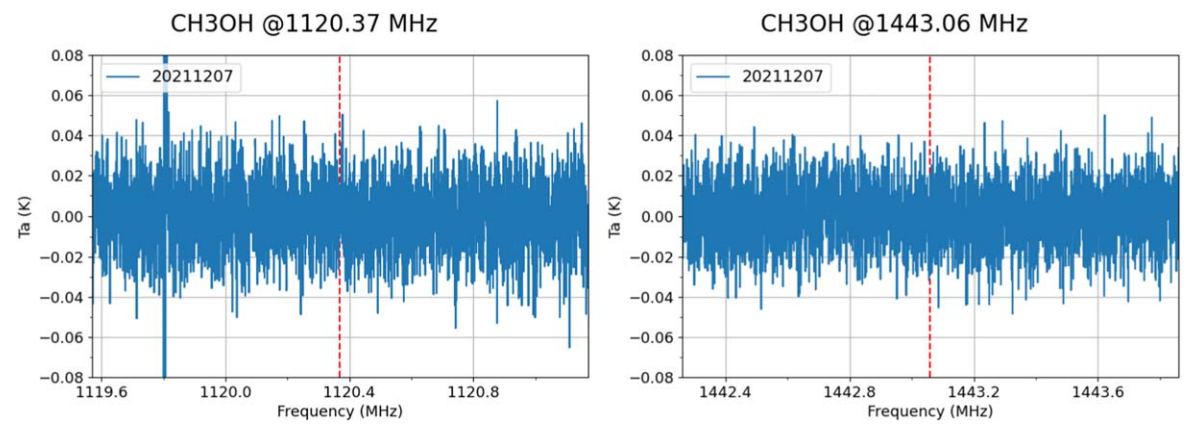


Figure 4. The spectra of comet C/2021 A1 (Leonard) obtained on 2021 December 07. The red vertical dashed lines mark the rest frequencies of CH₃OH. The upper and lower panels for CH₃OH at 1.120 and 1.443 GHz, respectively.

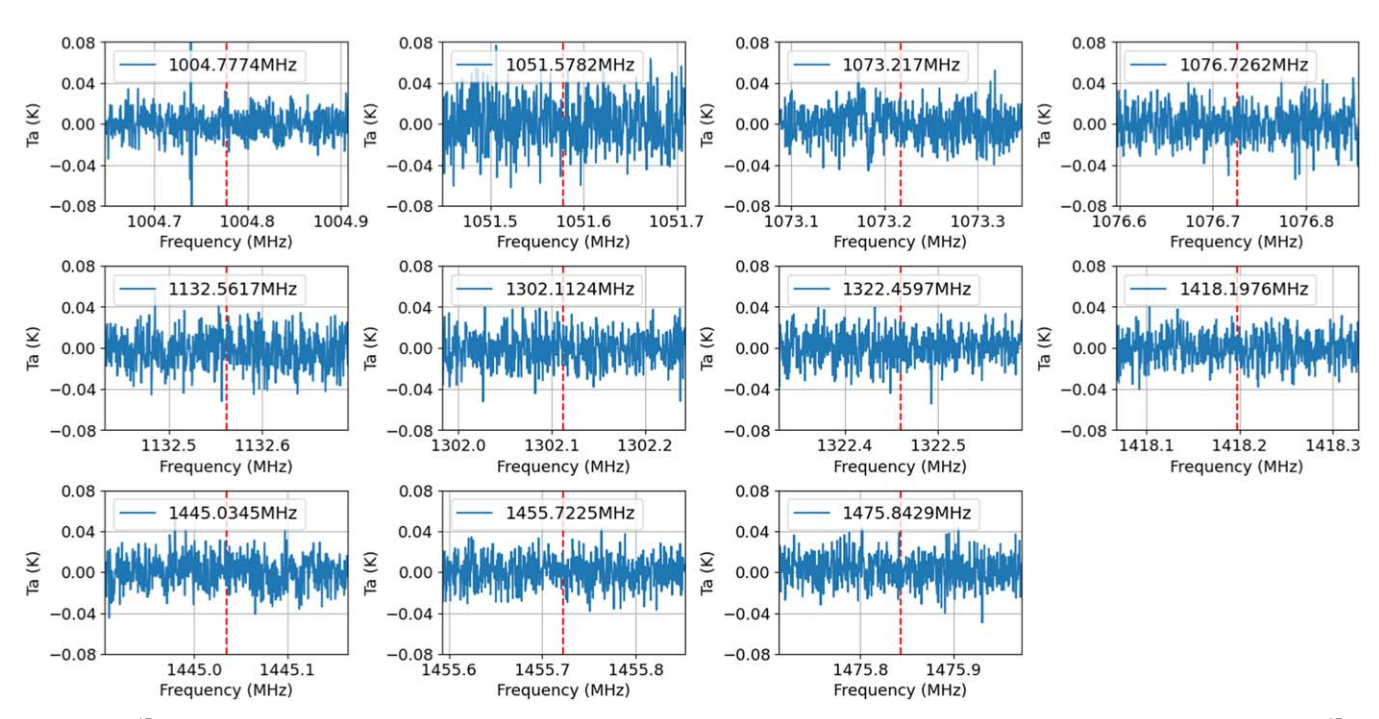


Figure 5. The ¹⁷OH spectra of comet C/2021 A1 (Leonard) obtained on 2021 December 07. The red vertical dashed lines mark the rest frequencies of ¹⁷OH.

feature near the expected transitions of 1073.214 MHz. Further inspection of the data suggests that this "absorption" resulted from the subtraction of the off-source spectrum from the on-source spectrum, which means that it is an emission both in the on-source and off-source spectra. Therefore, we conclude that this is an artifact due to RFI.

No observations were reported for the detection of ¹⁷OH in comets in the literature. To estimate the upper limit column density of ¹⁷OH, we assumed a line width of 2.5 km s⁻¹ based on the OH line profile for comet NEOWISE observed by

Arecibo (Smith et al. 2021). Since the excitation temperature of $^{17}\mathrm{OH}$ in comet comas is unknown, we simply adopted a range of values from 10 to 100 K and calculated the 3σ upper limit column density of $^{17}\mathrm{OH}$ at 1.302 GHz. It should be noted that the excitation temperature used here is not physically appropriate since the maser effects due to the absorption of solar radiation are very important for the OH excitation (Schleicher & A'Hearn 1988). Therefore, the above constraints on the $^{17}\mathrm{OH}$ column density are very crude. We found that the upper limit column density for $^{17}\mathrm{OH}$ is in the range of

 $7-10 \times 10^{12}$ cm⁻². The estimated value is about 2 times lower than the 16 OH column density previously reported (Smith et al. 2021).

In the cometary environments, the production of OH is dominated by the photodissociation of H_2O . The molecule ^{17}OH would be produced by the photodissociation of the isotopologue of water, H_2^{17} O. The oxygen isotopic abundance ratio of $^{17}O/^{16}O$ as derived from H_2^{17} O/ $H_2^{16}O$ in comet 67P/C-G is $\sim 4 \times 10^{-4}$ (Altwegg et al. 2015; Müller et al. 2022). If we assume the same abundance ratio of $^{17}OH/^{16}OH$ for comet NEOWISE and 67P/C-G, then that would indicate that our upper limit column density of ^{17}OH is highly overestimated. This suggests that the integrated intensity of ^{17}OH used in the calculations, i.e., the rms noise level with the current integration time is too high to constrain the signal strength of ^{17}OH . This also indicated that the non-detection of ^{17}OH is consistent with the expected $^{17}O/^{16}O$ elemental ratio.

Instead of constraining the molecular column density or production rate, we can use the molecular production rate reported in the literature to estimate the expected integrated intensity of *L*-band molecular emissions. The molecular production rate can be expressed by the following Equation (2), assuming optically thin and LTE (Drahus et al. 2010),

$$Q = \frac{2}{\sqrt{\pi \ln 2}} \frac{k_B}{h} \frac{b \Delta v_{\text{exp}}}{DI(T)\nu} (e^{h\nu/k_B T} - 1) \int T_{mb} d\nu, \qquad (2)$$

where Q is the production rate in molecules per second, k_B and h are Boltzmann constant and Planck constant, respectively, b = 1.2 is the dimensionless factor of the full width at half maximum (FWHM) of the telescope's beam, D is the antenna's aperture, Δ is the geocentric distance of the comet, $v_{\rm exp}$ is the expansion velocity of gas, ν and I(T) are the rest frequency of the molecule and line intensity at temperature T, respectively, and $\int T_{mb} dv$ is the integrated intensity. Using the production rates of molecules reported for comets in the literature, we can derive the intensity of molecular emissions. Table 4 shows the estimated integrated intensity for CH₃OH at 1.443 GHz and ¹⁷OH at 1.302 GHz for comets NEOWISE, 67P/C-G, and C/2021 A1 (Leonard), which have the production rates for CH₃OH and OH previously reported. It should also be noted here that these estimations are based on the LTE assumption, so the results are rough estimates. The maser effects or non-LTE assumption should be considered if one wants to obtain a more accurate estimate. The integrated intensity for OH at 1.667 GHz is also estimated for comparison. The estimated integrated intensity for CH₃OH at 1.443 GHz and ¹⁷OH at 1.302 GHz are orders of magnitude lower than that for OH at 1.667 GHz. Therefore, we do not expect the detection of those molecular lines in the L-band in

our data, at least for CH₃OH and ¹⁷OH. The possible reasons are discussed in the following section.

Except for CH_3OH and ^{17}OH , there are various other molecules whose transition lines fall in the L-band. Table 5 lists a subset of molecules of interest. None of these molecules were identified, and their detection thresholds are far below the limit of current constraints. Several reasons can lead to the non-detection. Apart from CH_3OH or H_2CO , whose abundances are a few to ten percent relative to water, for other molecules, such as C_2H_5OH shown in the list, their abundances relative to water could be lower than one percent. On the other hand, large molecules tend to have more transition lines. However, due to the energy distribution in these lines, the intensity for transition lines at L-band is weaker than the high-frequency lines. The non-LTE effects for the molecule excitation in the cometary coma environment may also complicate the situation (Bockelée-Morvan et al. 2004).

Finally, we examined the potential line features of CH₃OH, ¹⁷OH, and other molecules for the comets C/2020 R4 (ATLAS) and C/2020 F3 (NEOWISE). However, the RFI was more severe in the data obtained before 2021 November because the electronic environment of the FAST feed cabin was not improved until after that time. Therefore, fewer RFI-free bands in the 1.0–1.5 GHz were available for these two comets. In summary, we did not identify convincing molecular emission signals in the observations for these comets, either.

3.2. The Neutral Hydrogen Line

Since our primary scientific goal is to search the molecular lines, we did not specifically consider the background contamination of comets when scheduling our observation plans, which is important if we want to identify the HI emission from the comet itself. We have visually checked the background contamination by stacking the comets' position and the HI4PI survey (HI4PI Collaboration et al. 2016). We found that, for comet NEOWISE and the last two scheduled observations of comet C/2020 R4 (ATLAS), the background was clean. While for other comets during their observations. they either coincide with a background cloud or on the edge of a background cloud, thus unsuitable for constraining the HI emission from those comets. As a result, the HI spectrum from comet 67P/C-G, C/2021 A1 (Leonard), and C/2020 R4 (ALTAS) have a complex profile with multiple components, likely due to the background contamination. Most importantly, the off-source positions were also characterized by similar HI spectrum, thus we were also unable to perform a good baseline subtraction.

For comet NEOWISE, although it was visually located in a clean background during its observations, there were still H I emissions around 1420.4 MHz both from the on-source

Table 4
The Estimated Integrated Intensity for Molecular Lines of CH₃OH (at 1.443 GHz), ¹⁷OH (at 1.302 GHz), and OH (at 1.667 GHz) for Comets C/2020 F3 (NEOWISE), 67P/C-G, and C/2021 A1 (Leonard)

Comet Name	Molecule	Production Rate (molecules s ⁻¹)	Estimated Integrated Intensity (mK km s ⁻¹)
C/2020 F3 (NEOWISE)	CH₃OH ¹⁷ OH OH	1.25×10^{28} (Biver et al. 2022) 1.44×10^{25a} 3.6×10^{28} (Smith et al. 2021)	$ \begin{array}{c} 1.6 \times 10^{-4} \\ 1.7 \times 10^{-4} \\ 8.1 \end{array} $
67P/C-G	СН₃ОН ¹⁷ ОН ОН	3.67×10^{26} (Biver et al. 2023) 4.4×10^{24a} 1.1×10^{28} (Biver et al. 2023)	$6.4 \times 10^{-6} $ $4.9 \times 10^{-5} $ 2.4
C/2021 A1 (Leonard)	¹⁷ ОН ОН	3.7×10^{25a} 9.31×10^{28} (Skirmante & Jasmonts 2022)	$1.9 \times 10^{-3} \\ 94.6$

Note

position and off-position. The HI emission profile was less complicated than in the other scheduled observations of comets. Figure 6 shows the 20 minutes of integration of the H I emission for the on-source position and off-position without Doppler correction from comet NEOWISE. Due to the different total on-source and off-source times for comet NEOWISE, we were unable to give a baseline subtraction from the off-source. It was also noted from Figure 6 that off-source HI emission was slightly stronger than the on-source HI emission by less than 1 K. The calculated H I column density is 1.5×10^{20} cm⁻² and 1.9×10^{20} cm⁻² for the on-source and off-source positions, respectively. This difference could be due to the spatial variation of background HI gas. On the other hand, due to the large FAST beam size (174") and small comet nucleus size (0"009) at the observed distance, the obstruction of background emission by the comet could be ignored. Therefore, from these observations, we could not constrain whether comet NEOWISE has an HI emission or not.

To our best knowledge, there is almost no report of H I in the radio wavelength range for comets to date. Recently, Pal & Manna (2024) reported an H I absorption detection from comet NEOWISE using the Giant Metrewave Radio Telescope (GMRT), and derived an H_I column density on the order of 10²¹ cm⁻². If we simply assume that H I and OH are mainly produced by the photodissociation of H₂O, then the production rate and column density for HI and OH should be similar. Keller & Lillie (1974) reported such a similar production rate for HI and OH with no less than 2 times difference for the comet Bennett (1970 II). For comet NEOWISE, compared with the derived OH column density of $1.1 \times 10^{13} \, \text{cm}^{-2}$ from Smith et al. (2021), the derived H I column density from Pal & Manna (2024) was highly overestimated. From our observations, although the dip around 1420.4 MHz may be interpreted as an absorption feature from the on-source spectrum, we could not

rule out the possibility of the multi-components of emission feature when compared with the off-source profile. Moreover, if we assume that the production rate for H I is comparable with that of OH, the integrated line intensity for H I would be below our detection limit.

4. Discussion

Molecules in the coma originate from the outgassing of the nucleus, sublimation of ice species in the coma, or formed directly in the coma by photochemical processes (Cordiner et al. 2023). The chemical composition of comets is essential to study the chemical inheritance from the protosolar nebula to the planetary system. Both in situ measurements and remote observations are used to identify the molecular species in comets. Numerous molecules have been discovered in Jupiterfamily comet 67P/C-G, mainly due to the Rosetta mission of the European Space Agency. On the other hand, molecules in many long-period Oort Cloud comets have been observed during their perihelion passages by remote observations in the optical, infrared, or radio wavelengths. Table 6 summarizes the detected molecules reported in the literature for the four comets we observed as derived from observations in various wavelengths.

The detectability of molecules depends on the activity of the comet. Molecules in highly active comets are relatively easy to detect (Biver et al. 2015; Protopapa et al. 2021; Faggi et al. 2023). Volatile species can be released during the sublimation of H_2O and CO_2 ices (Rubin et al. 2023), which is a consequence of the outburst due to the thermodynamic evolution of the cometary nucleus surface and subsurface layers (Wesołowski 2022). Astrochemical models also show that abundant organic molecules can be present in the coma due to the outgassing of the nucleus and gas-phase chemistry in the

^a Assuming $Q(^{17}OH) = 4 \times 10^{-4} Q(OH)$.

Table 5
A Subset of Molecules of Interest Used for Searching in This Study

Groups	Molecules
P-bearing molecules	PO, PH ₃
S-bearing molecules	SH, H ₂ CS, H ₂ SO ₄
Carbon-chains	C ₆ H, C ₉ H, C ₆ O, C ₇ O, C ₉ O, HC ₇ N, HC ₉ N, HC ₁₁ N
Complex organic molecules	$CH_3OH,\ CH_3CHO,\ CH_3COOH,\ CH_3CH_2CHO,\ C_2H_5OH,\ C_2H_5CN,\ NH_2CH_2CH_2OH,\ H_2NCH_2COOH-II,\ H_2NCH_2COOH-II,\ a'GG'g-CH_2OHCH_2CH_2OH,\ aG'g-CH_3CHOHCH_2OH$
Others	¹⁷ OH, ¹⁸ OH, OD, H ₂ CO, D ₂ CO, NO, NH ₃ , ND ₃

Table 6
Summary of the Molecules Detected by Ground-based Observations in the Optical, Infrared, and Radio Wavelengths for Comets C/2020 F3 (NEOWISE), C/2020 R4 (ATLAS), 67P/C-G, and C/2021 A1 (Leonard)

Comet	Wavelength	Detected Molecules	References
C/2020 F3 (NEOWISE)	optical	CN, CH, C ₂ , C ₃ , NH ₂ , CO ⁺ , H ₂ O ⁺ , N ₂ ⁺ , CO, OCS, HCN, C ₂ H ₂ , NH ₃ , H ₂ CO, CH ₄ , C ₂ H ₆ , CH ₃ OH	(1, 2, 3, 4)
	infrared	CN, NH ₂ , OH, H ₂ O, HCN, NH ₃ , CO, C ₂ H ₂ , C ₂ H ₆ , CH ₄ , CH ₃ OH, H ₂ CO	(5)
	radio	OH, HCN, HNC, CH ₃ OH CS, H ₂ CO, CH ₃ CN, H ₂ S, CO	(6, 7, 8)
C/2020 R4 (ATLAS)	optical	CN, NH, C ₂ , C ₃	(9)
67P/C-G	radio	OH, HCN, CH ₃ OH, H ₂ S, CS, CH ₃ CN, H ₂ CO, HNCO, H ₂ O	(10)
C/2021 A1 (Leonard)	optical	NH ₂ , C ₂	(11)
	infrared	H ₂ O, HCN, NH ₃ , CO, C ₂ H ₂ , C ₂ H ₆ , CH ₄ , CH ₃ OH, H ₂ CO, OCS, HCl, CN, NH ₂ , OH	(12)
	radio	OH, HCN, HNC, CS, OCS, H_2S , H_2CO , HCOOH, HNCO, HC ₃ N, CH ₃ CN, NH ₂ CHO, CH ₂ CO, CH ₃ OH, CH ₃ CHO, CH ₂ OHCHO, C ₂ H ₅ OH, (CH ₂ OH)2	(13, 14)

Note. (1) Cambianica et al. (2021a), (2) Cambianica et al. (2021b), (3) Faggi et al. (2020), (4) Munaretto et al. (2023), (5) Faggi et al. (2021), (6) Smith et al. (2021), (7) Biver et al. (2022), (8) Drozdovskaya et al. (2023), (9) Manzini et al. (2021), (10) Biver et al. (2023), (11) Mugrauer (2021), (12) Faggi et al. (2023), (13) Skirmante & Jasmonts (2022), (14) Biver et al. (2024).

coma (Cordiner & Charnley 2021; Ahmed & Acharyya 2022). For the four comets that we observed, C/2020 R4 (ATLAS) was observed by only optical facilities. Lin et al. (2021) found at least three outbursts in their observations and did not see any new jet features and fragments based on its coma morphology. For comet NEOWISE and 67P/C-G, although multiple molecules have been observed in the frequency range higher than 100 GHz by IRAM 30 m radio telescope and NOEMA interferometry array, OH is the only molecule detected in the low-frequency *L*-band. Comet C/2021 A1 (Leonard) was observed by FAST about one month before its perihelion, although many volatile species were detected in the near-infrared range two weeks before the perihelion (Faggi et al. 2023).

In the previous section, the LTE condition was assumed to calculate the molecular production rates. However, in the cometary coma environment, the LTE condition may not be valid due to the processes of various other excitation mechanisms (Bockelée-Morvan et al. 2004). For example,

although OH could be excited by the 2.7 K background radiation, the dominated mechanism to excite OH is the resonance fluorescence by the absorption of solar radiation (Schleicher & A'Hearn 1988). Therefore, the non-detection of radio wavelength of *L*-band molecular lines in the cometary environment could rule out the possibility of anomalously strong lines, which would be caused by pumping of ultraviolet/infrared radiation or other non-LTE effects.

In addition to the production rates of molecules, the detectability of molecules in the radio wavelengths depends on their intrinsic transitional characteristics and environmental excitation conditions, such as the Einstein A-coefficient and upper/lower energy at a specific level of excitation, as well as the gas temperature and number density of molecules in the coma. For the detection of more than 300 molecules in the ISM, ¹⁶ the observed frequencies are in the range of tens to hundreds of GHz, and most of them are in star-forming regions

https://cdms.astro.uni-koeln.de/classic/molecules

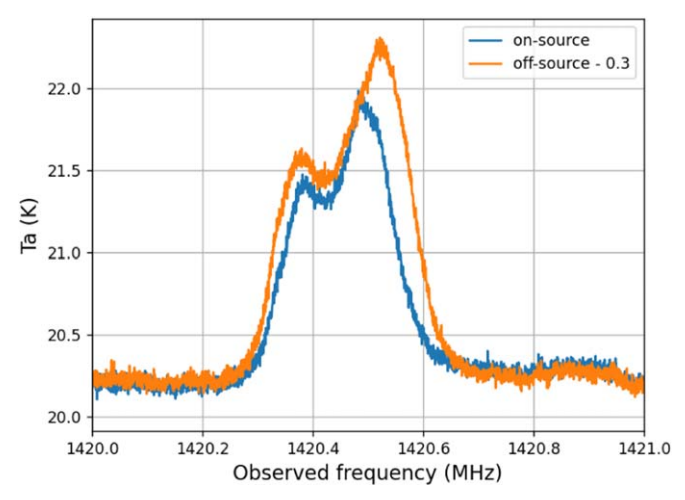


Figure 6. The 20 minutes of integration of H I emission both for the on-source and off-source position during the observations of comet NEOWISE.

(McGuire 2022), suggesting that the excitation conditions of molecules are related to their environment. Although many molecular transitions fall in the L-band, including the organic and prebiotic molecules, the high upper-level energy ($E_{\rm up}$) and/or low value of Einstein A-coefficient (A_{ij}) of the molecular excitation conditions do not favor their detection in the L-band in the cometary environment. For example, methanol, one of the molecules commonly detected in comets with high-frequency transitions, has $E_{\rm up}$ and A_{ij} generally several of tens Kelvin and higher than $10^{-6}~{\rm s}^{-1}$, respectively. However, the highest A-coefficient for molecules in the L-band is less than $10^{-9}~{\rm s}^{-1}$, and the $E_{\rm up}$ can be as high as hundreds of Kelvin, making the detection much harder than in the high-frequency bands.

Finally, in the *L*-band, RFI is usually more severe than at high frequencies and has to be considered in data analysis. The wide frequency range of RFI reduces the usable frequency bandwidth and introduces ambiguities in the identifications of molecular spectral lines. The ultra-wide bandwidth receiver (Zhang et al. 2023), which will cover the 0.5–3.3 GHz frequency range, once installed on FAST, could greatly benefit the detection of molecules in comets.

5. Summary

We observed four comets, C/2020 F3 (NEOWISE), C/2020 R4 (ATLAS), C/2021 A1 (Leonard), and 67P/Churyumov-Gerasimenko, to detect their molecular emission or absorption features in the radio L-band from 1.0 to 1.5 GHz using FAST from 2020 August to 2021 December. We searched for thousands of line transitions associated with hundreds of molecular species in the RFI-free frequency channels in the data. No clear evidence of the emission lines was present, resulting in a null detection of those molecules in these four comets. Under the LTE conditions, we estimated the integrated

intensity for CH₃OH at 1.443 GHz and ¹⁷OH at 1.302 GHz using their production rates reported in the literature, and found that the expected intensity for the searched molecular lines is too weak to be detected in our observations. Therefore, it is not surprising for the non-detection of molecular lines in the *L*-band from 1.0 to 1.5 GHz. This non-detection of molecular lines in the cometary environment could also rule out the possibility of unusually strong lines. Observing highly active comets and the implementation of the ultra-wide bandwidth receiver on FAST expected in the near future will improve the detectability of molecular lines in comets.

Acknowledgments

We thank the reviewer for the suggestions that helped us greatly improve the manuscript. The authors thank Qingliang Yangand Chun Sun at FAST Operation Center for assisting in the development of the special observation mode for moving target observations. The authors would also like to express great gratitude to Zhong-Yi Lin and Wing-Huen Ip for their generous suggestions and valuable discussions regarding this project. This work is supported by a grant from the National Natural Science Foundation of China (NSFC) No. 11988101. L.-F.C. acknowledges the support from the China Postdoctoral Science Foundation grant No. 2023M733271 and the Foundation of Education Bureau of Guizhou Province, China (grant No. KY (2020) 003). C.-W.T. is supported by the International Partnership Program of the Chinese Academy of Sciences, program No. 114A11KYSB20210010. Z.P. and L.Q. acknowledge the support from the National Key R&D Program of China grant Nos. 2022YFC2205202 and 2020SKA0120100, and by the NSFC grant Nos. 11703047, 11773041, U2031119, 12173052, 12173053, 12373032, and 11963002. Z.P. and L.Q. are supported by the CAS "Light of West China" Program and the Youth Innovation Promotion Association of the Chinese Academy of Sciences (ID Nos. 2023064, 2018075, and Y2022027). D.L. is a New Cornerstone Investigator. D.Q. and X.-J.J. acknowledge the support by the NSFC grant No. 12373026.

ORCID iDs

Ruining Zhao https://orcid.org/0000-0003-4936-4959 Pei Zuo https://orcid.org/0000-0003-3948-9192

References

```
Ahmed, S., & Acharyya, K. 2022, arXiv:2207.13288K.
Altwegg, K., Balsiger, H., Bar-Nun, A., et al. 2015, Sci, 347, 1261952
Altwegg, K., Balsiger, H., Bar-Nun, A., et al. 2016, SciA, 2, e1600285
Bauer, J., Gicquel, A., Kramer, E., et al. 2020, AAS/DPS Meeting, 52, 316.04
Bergman, P., Lerner, M. S., Olofsson, A. O. H., et al. 2022, A&A, 660, A118
Bergner, J. B., & Ciesla, F. 2021, ApJ, 919, 45
Biver, N., & Bockelée-Morvan, D. 2019, ESC, 3, 1550
Biver, N., Bockelée-Morvan, D., Crovisier, J., et al. 2023, A&A, 672, A170
Biver, N., Bockelee-Morvan, D., Handzlik, B., et al. 2024, arXiv:2408.10759
Biver, N., Bockelée-Morvan, D., Moreno, R., et al. 2015, SciA, 1, 1500863
Biver, N., Boissier, J., Bockelée-Morvan, D., et al. 2022, A&A, 668, A171
Bockelée-Morvan, D., Crovisier, J., Mumma, M. J., & Weaver, H. A. 2004, in
   Comets II, ed. M. C. Festou, H. U. Keller, & H. A. Weaver, 391 (Tucson:
   Univ. Arizona Press)
Brasser, R., & Morbidelli, A. 2013, Icar, 225, 40
Cambianica, P., Cremonese, G., Munaretto, G., et al. 2021a, EPSC, EPSC2021,
   EPSC2021-523
Cambianica, P., Cremonese, G., Munaretto, G., et al. 2021b, A&A, 656, A160
Chambers, J. 2023, ApJ, 944, 127
Cordiner, M. A., & Charnley, S. B. 2021, MNRAS, 504, 5401
Cordiner, M. A., Roth, N. X., Milam, S. N., et al. 2023, ApJ, 953, 59
Drahus, M., Küppers, M., Jarchow, C., et al. 2010, A&A, 510, A55
Drozdovskaya, M. N., Bockelée-Morvan, D., Crovisier, J., et al. 2023, A&A,
   677, A157
Ehrenfreund, P., & Charnley, S. B. 2000, ARA&A, 38, 427
Faggi, S., Lippi, M., Camarca, M., et al. 2021, AJ, 162, 178
Faggi, S., Lippi, M., Mumma, M. J., & Villanueva, G. L. 2023, PSJ, 4, 8
Faggi, S., Mumma, M., Villanueva, G., & Lippi, M. 2020, AAS/DPS Meeting,
   52, 111.01
Giorgini, J. D., Yeomans, D. K., Chamberlin, A. B., et al. 1996, AAS/DPS
   Meeting, 28, 25.04
HI4PI Collaboration, Bekhti, B., Flöer, N., et al. 2016, A&A, 594, A116
Jiang, P., Tang, N.-Y., Hou, L.-G., et al. 2020, RAA, 20, 064
Keller, H. U., & Lillie, C. F. 1974, A&A, 34, 187
```

```
Leonard, G. J., Aschi, S., Pettarin, E., et al. 2021, MPEC, 2021, A99
Li, D., Wang, P., Qian, L., et al. 2018, IMMag, 19, 112
Lin, Z.-Y., Kelly, M. S. P., & Ip, H.-W. 2021, EPSC, EPSC2021, EPSC2021-448
Lovell, A. J., Howell, E. S., Schloerb, F. P., Lewis, B. M., & Hine, A. A. 2002,
  in ESA SP, Asteroids, Comets, and Meteors: ACM 2002, ed. B. Warmbein
  (Noordwijk: ESA Publications Division), 681
Manzini, F., Ochner, P., Oldani, V., & Bedin, L. R. 2021, ATel, 14585, 1
McGuire, B. A. 2022, ApJS, 259, 30
Mugrauer, M. 2021, ATel, 15119, 1
Müller, D. R., Altwegg, K., Berthelier, J. J., et al. 2022, A&A, 662, A69
Munaretto, G., Cambianica, P., Cremonese, G., et al. 2023, P&SS, 230, 105664
Nan, R., Li, D., Jin, C., et al. 2011, IJMPD, 20, 989
Pal, S., & Manna, A. 2024, JApA, 45, 10
Pan, Z., Ma, X.-Y., Qian, L., et al. 2021, RAA, 21, 143
Protopapa, S., Kelley, M. S. P., Woodward, C. E., & Yang, B. 2021, PSJ,
  2, 176
Qian, L., & Pan, Z.-C. 2021, RAA, 21, 185
Qian, L., Yao, R., Sun, J., et al. 2020, Innov, 1, 100053
Roth, N. X., Milam, S. N., Cordiner, M. A., et al. 2021, PSJ, 2, 55
Rubin, M., Altwegg, K., Berthelier, J.-J., et al. 2023, MNRAS, 526, 4209
Rubin, M., Bekaert, D. V., Broadley, M. W., Drozdovskaya, M. N., &
   Wampfler, S. F. 2019, ESC, 3, 1792
Salter, C. J., Ghosh, T., Catinella, B., et al. 2008, AJ, 136, 389
Schleicher, D. G., & A'Hearn, M. F. 1988, ApJ, 331, 1058
Shu, F. H. 1977, ApJ, 214, 488
Skirmante, K., & Jasmonts, G. 2022, A&AT, 33, 139
Smith, A. J., Anish Roshi, D., Manoharan, P., et al. 2021, PSJ, 2, 123
Tan, W. S., Araya, E. D., Lee, L. E., et al. 2020, MNRAS, 497, 1348
Tremblay, C. D., Gray, M. D., Hurley-Walker, N., et al. 2020, ApJ, 905,
Tremblay, C. D., Hurley-Walker, N., Cunningham, M., et al. 2017, MNRAS,
  471, 4144
Tremblay, C. D., Jones, P. A., Cunningham, M., et al. 2018, ApJ, 860, 145
Tseng, W. L., Bockelée-Morvan, D., Crovisier, J., Colom, P., & Ip, W. H.
  2007, A&A, 467, 729
van Dishoeck, E. F., Herbst, E., & Neufeld, D. A. 2013, ChRv, 113, 9043
Wesołowski, M. 2022, RAA, 22, 055015
Willacy, K., Turner, N., Bonev, B., et al. 2022, ApJ, 931, 164
Zhang, C.-P., Jiang, P., Zhu, M., et al. 2023, RAA, 23, 075016
Zhang, Q., Ye, Q., Vissapragada, S., Knight, M. M., & Farnham, T. L. 2021,
   AJ, 162, 194
```